The Journal of Chemical Physics

Full-dimensional MRCI-F12 potential energy surface and dynamics of the $F(^2P_{3/2}) + C_2H_6 \rightarrow HF + C_2H_5$ reaction

Cite as: J. Chem. Phys. **153**, 064305 (2020); https://doi.org/10.1063/5.0018894
Submitted: 18 June 2020 . Accepted: 19 July 2020 . Published Online: 13 August 2020

Dóra Papp, and Gábor Czakó

The Journal of Chemical Physics ARTICLE scitation.org/journal/jcp

Full-dimensional MRCI-F12 potential energy surface and dynamics of the $F(^2P_{3/2}) + C_2H_6 \rightarrow HF + C_2H_5$ reaction

Cite as: J. Chem. Phys. 153, 064305 (2020); doi: 10.1063/5.0018894
Submitted: 18 June 2020 • Accepted: 19 July 2020 •
Published Online: 13 August 2020

Dóra Papp[a] and Gábor Czakó[a]

AFFILIATIONS

MTA-SZTE Lendület Computational Reaction Dynamics Research Group, Interdisciplinary Excellence Centre and Department of Physical Chemistry and Materials Science, Institute of Chemistry, University of Szeged, Rerrich Béla tér 1, Szeged H 6720, Hungary

[a]Authors to whom correspondence should be addressed: dorapapp@chem.u-szeged.hu and gczako@chem.u-szeged.hu

ABSTRACT

We report a detailed quasi-classical dynamics study on a new full-dimensional multireference spin–orbit-corrected potential energy surface (PES) for the $F(^2P_{3/2}) + C_2H_6 \rightarrow HF + C_2H_5$ reaction. For the PES development, the Robosurfer program package is applied and the MRCI-F12+Q(5,3)/aug-cc-pVDZ energy points are fitted using the monomial symmetrization approach of the permutationally invariant polynomial method. Our simulations provide substantial reaction probabilities and sharply increasing cross sections with an increase in collision energy for this early- and negative-barrier reaction. A direct rebound/stripping mechanism is preferred at low/high collision energies, and the initial translational energy turns out to convert mostly into product recoil, whereas the reaction energy excites the HF vibration. Vibrational and vibrationally resolved rotational state distributions of the HF product obtained from our computations agree well with the single-collision experimental data for the $v_{HF} = 1$, 2, and 3 states.

I. INTRODUCTION

Following the detailed dynamical investigations of the atom + diatom reactive systems, going back to the 1970s,[1–5] the size of the studied chemical reactions grew by one atom on average per decade. The basic rules of chemical dynamics have also been established by John Polanyi for the A + BC reactions,[6] saying that the translational energy is more efficient in promoting the chemical reactions having reactant-like transition states (early-barrier reactions) than the vibrational excitation of the BC bond, and the reverse is true when the transition state is product-like (late-barrier reactions). Based on the in-depth analysis of the atom + H_2O[7–11] and the atom + CH_4[12–29] benchmark reactions featuring more and more complex dynamical behavior, the Polanyi rules have later been extended and new laws of polyatomic reactivity have been set up.[16–18,23] The progress of the field of chemical dynamics has always been stimulated by the close collaboration between theory and experiment; however, the experimental techniques turned out to be more feasible in the case of larger systems[30–35] than the accurate computational methods of dynamics investigations. In theoretical simulations, first the potential energy surface (PES) of the system has to be known, which provides the gradients, and thereby the governing forces in classical, or the potential energy operator in quantum dynamics computations describing the motion of the atoms in the reaction. Although simulations using semiempirical or lower-level *ab initio* methods to represent the PESs have been carried out,[36,37] the accurate description using the state-of-the-art techniques of the electronic structure theory of larger systems had to be waited for.

By this time, jumping three atoms within a decade, the theory has arrived to the point where it is capable of performing accurate dynamics simulations of even nine-atomic systems, first carried out by the present authors for the $Cl + C_2H_6 \rightarrow HCl + C_2H_5$ reaction providing unprecedented agreement with experiment for

the rotational state distribution of the HCl product.[38] The dynamics of another chemical reaction of this size is under theoretical investigation in this study: the F + C_2H_6 → HF + C_2H_5 reaction, featuring an entirely different potential energy landscape with a reactant-like transition state[39] with respect to the slightly late- or central-barrier Cl + C_2H_6 → HCl + C_2H_5 reaction, and posing challenges of the quantum chemical description of its entrance channel. The F + C_2H_6 → HF + C_2H_5 reaction has already been the subject of both experimental[35,40–43] and theoretical[37,39,44–46] studies. The experiments investigating the kinetics of the title reaction have provided contradictory results regarding the Arrhenius-[40,43] or non-Arrhenius-like[41,42] behavior of the reaction. Nesbitt and co-workers later carried out single-collision experiments using high-resolution infrared laser absorption methods providing detailed state-to-state dynamics of the F + C_2H_6 → HF + C_2H_5 reaction.[35] Theoretical investigations began with the characterization of the transition state and the reaction enthalpy of the title reaction using MP2 and CCSD(T) *ab initio* methods, and the calculation of rate constants, which strengthened its standard Arrhenius-like temperature dependence.[44] Later, Troya and co-workers studied the reaction by direct-dynamics methods (where the gradients of the PES are computed on-the-fly) using a semiempirical Hamiltonian.[37] Recently, Espinosa-Garcia *et al.* have developed a force-field-based PES for the F + C_2H_6 → HF + C_2H_5 reaction and performed kinetics calculations reporting also an Arrhenius-like behavior.[45] They also performed quasi-classical dynamics simulations investigating the rovibrational distribution of the HF product and the role of the ethyl radical[46] and very recently carried out ring polymer molecular dynamics computations for the reaction as well.[47] As an initial step for the dynamics study reported here, the present authors determined benchmark geometries and energies for the stationary points of the F + C_2H_6 reaction considering also the H-substitution and the methyl-substitution reaction pathways.[39]

In this study, we report a full-dimensional *ab initio* PES for the F + C_2H_6 → HF + C_2H_5 H-abstraction reaction developed using a multireference method to provide a correct description of the entrance channel, and, for the first time, we take spin–orbit coupling explicitly into account in our computations. Using this PES, we carry out quasi-classical trajectory (QCT) simulations, and discuss detailed dynamics results of the title reaction with comparison of the computed rovibrational distributions of the HF product to the experimental data taken from Ref. 35.

II. COMPUTATIONAL DETAILS

A. Potential energy surface development

As a first step of the PES development, the Cartesian coordinates of the stationary points[39] of the F + C_2H_6 reaction are randomly displaced in the 0 Å–0.4 Å interval and the reactants and products are randomly scattered around each other in the range of 3 Å–8 Å. Due to the high multireference character of the entrance-channel geometries caused probably by the effect of charge-transfer processes near the transition state,[48,49] the energies of the randomly generated initial geometry set are computed using a three-state MRCI-F12+Q(5,3)[50] explicitly-correlated multireference configuration–interaction method with the aug-cc-pVDZ basis set[51] augmented with relativistic spin–orbit (SO) correction determined based on the Breit–Pauli operator in the interacting-states approach.[52] During the MRCI-F12 computations a minimal active space of 5 electrons on 3 spatial 2p-like orbitals is used, and the Q Davidson-correction[53] estimates higher-order electron correlation effects. The spin–orbit eigenstates are determined by diagonalizing the 6 × 6 SO matrix whose diagonal elements are replaced by the Davidson-corrected MRCI-F12 energies. All quantum chemical computations utilize the MOLPRO program package.[54] After the single-point energy computations at the random geometries using the above-described level of theory, the initial dataset is cut by excluding geometries with energies higher than 100 kcal/mol relative to the global minimum of the set.

The iterative improvement of this initial potential energy surface is carried out by using the ROBOSURFER program package[55] developed recently in our group. A hard upper energy limit of 100 kcal/mol above the reactants is applied, and a hard lower limit of 50 kcal/mol below the reactants is also set to avoid spurious minima. The fitting of the energy points is performed within the framework of the monomial symmetrization approach (MSA)[56] of the permutationally invariant polynomial method,[57,58] i.e., using a full-dimensional analytical function that is invariant under the permutation of like atoms. This function is constructed as an expansion of polynomials of the $y_{ij} = \exp(-r_{ij}/a)$ Morse-like variables, where r_{ij} are the atom–atom distances and a, a parameter controlling the asymptotic behavior of the PES, is 1.5 bohr. The highest total polynomial order used in the fitting function is 5. The fitting is processed using a least-squares fit with a weighting factor $E_0/(E + E_0)$, where E is an energy relative to the global minimum of the fitting set, and $E_0 = 0.04$ hartree. The fifth order expansion requires 3234 fitting coefficients. A target accuracy of 0.5 kcal/mol is demanded up to 30 kcal/mol above the energy of the reactants during the development. New geometries are selected to improve the PES from QCT computations and in some iteration steps from the HOLEBUSTER[55] subprogram.

The development of the PES is performed at the above described MRCI-F12+Q(5,3)/aug-cc-pVDZ level of theory with the SO correction and consists of 111, 39, 5, and 50 ROBOSURFER iterations at collision energies 5 kcal/mol, 20 kcal/mol, 50 kcal/mol, and 20 kcal/mol, respectively, used in the QCT computations. In the last 50 iterations, the HOLEBUSTER subprogram is run and only a minimal amount of trajectories is computed. The final PES is built from 15 178 geometries and the corresponding SO-corrected MRCI-F12+Q(5,3)/aug-cc-pVDZ energies, and shows small root-mean-square (RMS) errors in the chemically interesting energy ranges (Table I).

TABLE I. Root mean square (RMS) errors in the chemically interesting regions of the PES (energy intervals are given relative to the global minimum of the fitting set).

Energy range (kcal/mol)	0–20	20–40	40–100
RMS error (kcal/mol)	0.39	0.52	1.04

B. Quasi-classical trajectory simulations

Quasi-classical dynamics simulations are carried out at collision energies 1.0 kcal/mol, 3.2 kcal/mol, 5.0 kcal/mol, 10.0 kcal/mol, and 20.0 kcal/mol for the $F(^2P_{3/2}) + C_2H_6 \rightarrow HF + C_2H_5$ reaction. At the beginning of the trajectories, the zero-point energy (ZPE) of ethane is set by standard normal-mode sampling.[59] The spatial orientation of the reactants is randomly sampled. The initial distance between the F atom and the center of mass of the ethane molecule is $\sqrt{x^2 + b^2}$, where $x = 16$ bohr and the impact parameter is varied between 0 and b_{max} (where the reaction probability vanishes) with a step size of 0.5 bohr. 1000 trajectories are run at each b value. At the collision energy of 1 kcal/mol, b_{max} is 8 bohr, and for all the other collision energies, it is 7 bohr, thus, the total number of trajectories is $(1 \times 17 + 4 \times 15) \times 1000 = 77\,000$. The trajectories are propagated with a 0.0726 fs time step until the largest interatomic distance becomes larger than the largest initial one by 1 bohr.

Integral cross sections (σ) for the title reaction are calculated by a b-weighted numerical integration of the $P(b)$ opacity functions at each collision energy,

$$\sigma = \pi \sum_{n=1}^{n_{max}} [b_n - b_{n-1}][b_n P(b_n) + b_{n-1} P(b_{n-1})], \quad (1)$$

where we divide the range $[0, b_{max}]$ into n_{max} equidistant parts with a width of 0.5 bohr, i.e., $b_n = 0.5n$ bohr, where $n = 0,1, \ldots, n_{max}$. For the products, different ZPE-constraints are set: (1) soft: those trajectories are discarded, where the sum of the classical vibrational energy of the C_2H_5 radical and the internal energy of the HF product is smaller than the sum of the harmonic ZPE of the ethyl radical corresponding to the present PES and the anharmonic ZPE corresponding to the actual rotational state of HF. The variationally determined rovibrational energy levels of the HF molecule are taken from Ref. 21. (2) Hard: those trajectories are discarded, where the classical vibrational energy of the C_2H_5 radical is smaller than its ZPE on the present PES *and* the internal energy of the HF product is also smaller than its ZPE corresponding to its actual rotational state. (3) ZPE constraint is only set for the C_2H_5 radical: its classical vibrational energy must be larger than its ZPE on the PES. The scattering angle distributions of the products are obtained by binning the cosine of the angle (θ) of the relative velocity vectors of the center of masses of the products and those of the reactants into 5 equidistant bins from -1 to 1. $\text{Cos}(\theta) = -1$ ($\theta = 180°$) corresponds to backward scattering. The rotational quantum number of the HF product is determined, as detailed in Ref. 38, and the vibrational quantum state of HF is obtained by finding the nearest variationally computed rovibrational energy level[21] corresponding to the actual rotational state of HF to the classical internal energy of HF. The experimental data for the vibrational distribution and the vibrationally-resolved rotational distributions of the HF product are taken from Ref. 35. The relative populations corresponding to both the theoretical and the experimental vibrationally-resolved rotational distributions are normalized so that their sum gives 1. For comparison with experiment, the most realistic theoretical results obtained from trajectories filtered by hard ZPE constraint are shown. In the case of the product scattering angle, translational, and internal energy distributions, no ZPE restriction is applied to show the qualitative behavior of these results with the best statistical accuracy.

III. RESULTS AND DISCUSSION

A. The potential energy surface

The schematic energy diagram of the $F(^2P_{3/2}) + C_2H_6 \rightarrow HF + C_2H_5$ reaction is shown in Fig. 1. The C_s-symmetry transition-state (TS) structure with a 141° bent C–H–F arrangement and with a large H–F distance of 1.94 bohr is clearly reactant-like.[39] The structure of the exit-channel minimum (postmin) is product-like with a short H–F bond length and an elongated C–H distance. The reaction is highly exothermic, in accordance with its early-barrier nature,[60] with a slightly submerged barrier and a deep post-reaction minimum. Figure 1 also shows the comparison of the classical relative energies of the stationary points of the title reaction obtained on the newly-developed PES, the SO-corrected MRCI-F12+Q(5,3)/aug-cc-pVDZ single-point energies computed at the geometries optimized on the PES, and the previously determined benchmark results.[39] The comparison of the former two indicates low (<0.4 kcal/mol) fitting errors of the full-dimensional PES, in consistence with the small RMS values of Table I. The relative energy of the TS obtained on the PES reproduces well the benchmark value (with only a 0.3 kcal/mol difference), thereby reflecting correctly its slightly submerged character. The adiabatic barrier height is also negative, −0.3 kcal/mol, relative to the reactants on the PES. The classical relative energies of the postmin structure and the products are about 2.5 kcal/mol higher than the benchmark energies, due probably to the somewhat weaker performance of the MRCI method with a minimal active space in the exit-channel; however, the level of theory used still preserves the energy gap between the exit-channel minimum and the product asymptote.

B. Reaction probabilities

Using the newly-developed PES, we carried out QCT simulations at five collision energies (1.0 kcal/mol, 3.2 kcal/mol, 5.0 kcal/mol, 10.0 kcal/mol and 20.0 kcal/mol) for the $F + C_2H_6 \rightarrow HF + C_2H_5$ reaction, and the opacity functions (reaction probabilities as a function of the impact parameter) obtained at the different

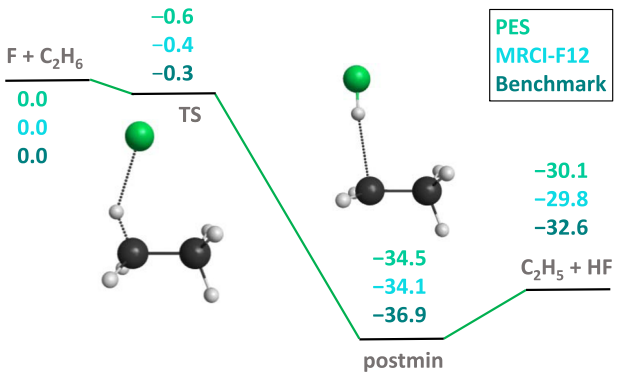

FIG. 1. Schematic potential energy diagram of the $F(^2P_{3/2}) + C_2H_6 \rightarrow HF + C_2H_5$ reaction comparing the classical relative energies obtained on the present PES, SO-corrected MRCI-F12+Q(5,3)/aug-cc-pVDZ single-point energies at geometries optimized on the PES, and the benchmark relative energies[39] of the stationary points.

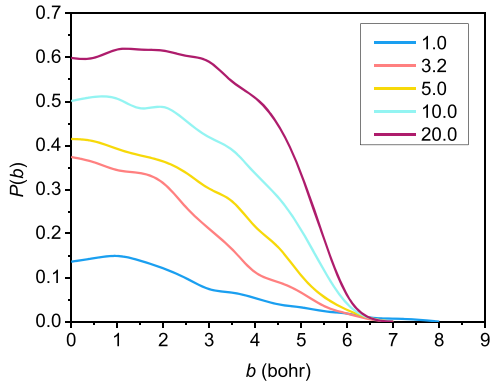

FIG. 2. Reaction probabilities as a function of the b impact parameter for the $F(^2P_{3/2}) + C_2H_6 \rightarrow HF + C_2H_5$ reaction at different collision energies (given in kcal/mol).

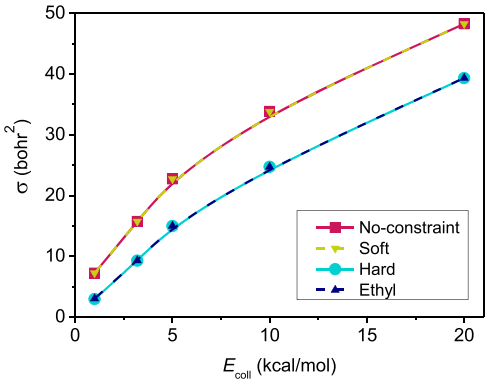

FIG. 3. Integral cross sections for the $F(^2P_{3/2}) + C_2H_6 \rightarrow HF + C_2H_5$ reaction as a function of the collision energy with different ZPE-constraints applied for the products (soft: the sum of the classical vibrational energies of the products is larger than the sum of their ZPEs, hard: the vibrational energy of each product molecule is larger than its ZPE, ethyl: ZPE constraint is set only for the ethyl radical).

collision energies are shown in Fig. 2. As seen in Fig. 2, no threshold energy above 1.0 kcal/mol can be observed for the title reaction to proceed, in accordance with the negative barrier height relative to the reactants. The increasing translational energy promotes the reaction very efficiently, from a probability of 15% at 1 kcal/mol to 60% at 20 kcal/mol collision energy at $b = 0$. As the collision energy increases, the reaction probabilities remain substantial also at larger b values with a faster decay near b_{max}, where the reaction probability becomes zero. This behavior indicates a direct rebound mechanism at low translational energies (occurring mainly at small impact parameters) and a stripping mechanism at higher collision energies (dominant at larger b values). The b_{max} value is the largest (8 bohr) at the lowest collision energy; otherwise, it shows no energy-dependence having the same value (7 bohr). The shape of the opacity functions is very similar to those observed for the $Cl + C_2H_6 \rightarrow HCl + C_2H_5$ reaction,[38] featuring also a slightly submerged barrier; however, for $Cl + C_2H_6$, the probabilities change in a narrower (25%–40%) range at $b = 0$, and a peak emerges with an increase in the translational energy at large b values, indicating the more pronounced presence of the stripping mechanism at high energies. The b_{max} values are somewhat larger for the $Cl + C_2H_6$ reaction, reaching even 11.5 bohr at 1 kcal/mol collision energy,[38] due presumably to the stronger dispersion interaction between the reactants. In the case of the $F + CH_4 \rightarrow HF + CH_3$ reaction,[21] where the barrier height is around zero with respect to the reactant asymptote, the reaction probabilities are in similar order of magnitude as in the $F/Cl + C_2H_6$ reactions and increase also with an increase in the collision energy. However, the opacity functions of the $F + CH_4$ reaction decay more rapidly at high translational energies, indicating a preference for the direct rebound mechanism.[21]

C. Excitation function

The excitation function [integral cross sections (ICSs) as a function of collision energy] of the title reaction, presented in Fig. 3, clearly reflects the highly efficient promotion of the reaction by the increase in the initial translational energy. This sharp increase in the cross sections with an increase in the collision energy, however, is in contrast with the findings for the $Cl + C_2H_6 \rightarrow HCl + C_2H_5$ reaction,[38] where the ICS decreases rapidly at low energies and moderately at higher energies. Both the F and $Cl + C_2H_6$ H-abstraction reactions feature slightly submerged barriers, although the transition-state geometries are entirely different.[39] Thus, in the case of the early-barrier $F + C_2H_6 \rightarrow HF + C_2H_5$ reaction, investing in translational energy increases the reactivity in accordance with the predictions of the Polanyi rules,[6] whereas it slightly hinders the late-/central-barrier $Cl + C_2H_6 \rightarrow HCl + C_2H_5$ reaction.[38] The $F + CH_4 \rightarrow HF + CH_3$ reaction, with a slightly positive spin–orbit-corrected barrier, also features an excitation function with a positive slope, without a threshold.[22]

Integral cross sections are also determined by applying different ZPE constraints for the products. Figure 3 shows that the soft restriction gives practically the same ICS values as if we did not apply any ZPE constraint, whereas the hard-constrained results are basically the same as those obtained with the ethyl-only ZPE constraint. The Polanyi rules predict for an early-barrier reaction that the diatomic product acquires considerable vibrational excitation due to the elongated bond-length at the transition-state geometry. Thus, if the soft restriction is set, the vibrational energy of the excited HF molecules will compensate that of the ZPE-violating ethyl radicals; thus, only very few trajectories will be discarded, resulting in qualitatively the same ICS determined without constraints. Accordingly, due probably also to this compensation, when we restrict only the vibrational energy of the ethyl radical, it gives basically the same results as the hard ZPE constraint. It is also shown in Fig. 3 that ZPE constraints make the ICS decrease significantly, but with a decreasing factor as the collision energy increases by 59%–18% from 1 kcal/mol to 20 kcal/mol.

D. Scattering angle distributions

Differential cross sections showing the scattering angle distributions of the title reaction are shown in Fig. 4. At low collision energies, backward scattering is preferred, indicating a direct

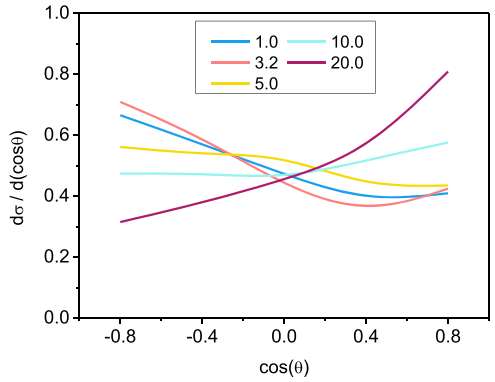

FIG. 4. Differential cross sections (obtained without ZPE constraint) showing the scattering angle (θ) distributions of the $F(^2P_{3/2}) + C_2H_6 \rightarrow HF + C_2H_5$ reaction at different collision energies (given in kcal/mol).

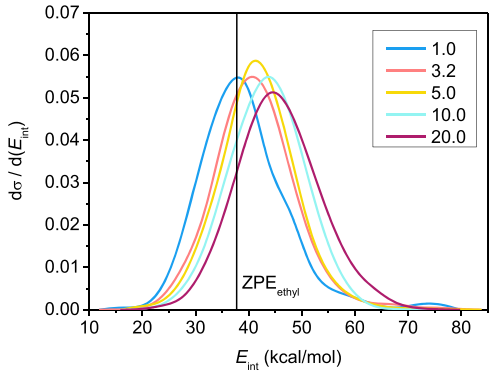

FIG. 6. Internal energy distributions of the C_2H_5 product (obtained without ZPE constraint) at different collision energies (given in kcal/mol). The vertical black line refers to the ZPE of the ethyl radical (37.8 kcal/mol).

rebound mechanism, while as the collision energy increases, the forward scattering stripping mechanism becomes dominant, in consistence with the shape of the opacity functions of Fig. 2. In the case of the $Cl + C_2H_6 \rightarrow HCl + C_2H_5$ reaction, the products at low collision energies are rather isotropically scattered,[38] suggesting a more indirect mechanism, which can be attributed to the more intense dispersion interaction between the reactants. In the case of the title reaction, the deep (with respect to the TS) exit-channel minimum also supports a direct mechanism because the energy gain from the transition state makes the system to promptly turn into products that are very close in energy.

E. The post-reaction distribution of energy

1. Relative translational energy of the products and internal energy of the ethyl radical

Differential cross sections showing the distribution of the relative translational energy of the products at different collision energies are plotted in Fig. 5. As shown in the figure, the distributions become broader as the collision energy increases, and their maxima are shifted by almost the total increment of the collision energy, indicating that the major part of the initial translational energy ends up in translational recoil in all cases. In consistence with this observation, the collision energy dependence of the internal energy distribution of the ethyl radical, plotted in Fig. 6, also suggests that only a small portion of the collision energy is transferred into the rotational or vibrational degrees of freedom of the ethyl fragment since the peaks of the distributions are not significantly affected by the change in the initial translational energy and are only slightly shifted from the ZPE of the ethyl radical. As shown in Fig. 6, a significant amount of the trajectories are ZPE-violating, especially at low collision energies, suggesting also that their energy is compensated by the high excitation of the HF product when soft ZPE constraint is applied (Fig. 3).

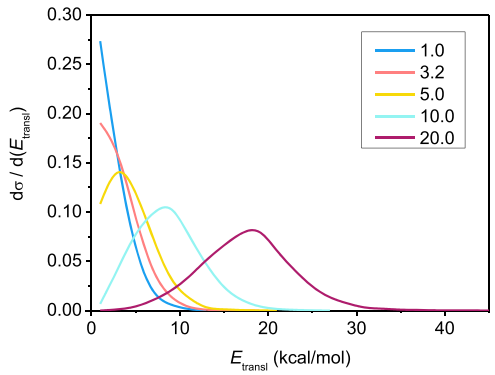

FIG. 5. Relative translational energy distributions (obtained without ZPE constraint) of the products of the $F(^2P_{3/2}) + C_2H_6 \rightarrow HF + C_2H_5$ reaction at different collision energies (given in kcal/mol).

2. Internal energy of the HF product, comparison with experiment

By analyzing the internal energy of the ethyl radical and the relative translational energy of the products, we conclude that the collision energy is mainly converted into product recoil, and only slightly into the rovibrational excitation of the ethyl product. Thus, practically no translational energy remains to excite the HF product molecule; however, the considerable reaction energy is retained for this purpose. As expected from the Polanyi rules, the HF product, indeed, forms in highly-excited vibrational states, as shown in Fig. 7, where the (hard-restricted) vibrational state distribution of the HF molecule is shown at different collision energies. The most populated state is $v = 2$, followed by $v = 3$ and $v = 1$, in decreasing order, while the vibrational ground state turns out to be very low-populated. The relative population of the vibrational states does not change significantly with the collision energy, confirming that the excitation energy is coming mostly from the reaction energy released, in consistence with the elongated H–F distance at the transition state.[17,49,61–64] However, at the highest collision energies, a small amount of the HF molecules is produced in the higher $v = 4$ state, indicating a non-negligible effect of the initial translational energy.

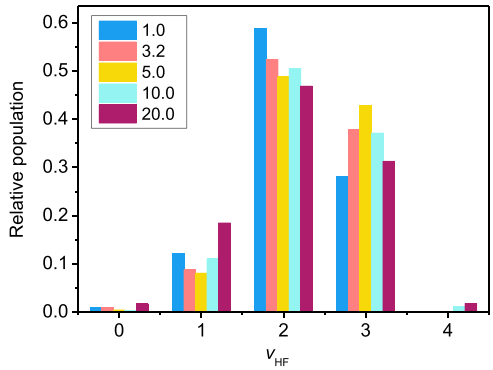

FIG. 7. Vibrational state distribution of the HF product at different collision energies (given in kcal/mol) when hard ZPE constraint (the vibrational energy of each product molecule must be larger than its ZPE) is applied for the products.

The vibrational state distributions of the HF molecule obtained with different product-ZPE constraints at 3.2 kcal/mol collision energy are shown in Fig. 8. The situation is similar here as in the case of the excitation function, that is, the no-constraint case is practically the same as if the soft restriction was set, which is no surprise because in the soft case, basically all trajectories are kept for analysis. In addition, Fig. 8 confirms the assumption that due to the highly-excited HF product molecules, the hard and "ethyl" ZPE constraints also discard practically the same trajectories, showing qualitatively the same vibrational distributions for the diatomic product. As shown in Fig. 8, restricting the ZPE of the ethyl radical affects significantly the relative populations of each vibrational state of HF, especially that of the $v = 1$ and $v = 2$ states, whose populations increase at the expense of the $v = 3$ fraction and of the vanishing population at $v = 4$.

A comparison of the vibrational state distribution of the HF product obtained from our simulations with the experimental data of Nesbitt and co-workers[35] at a collision energy of 3.2 kcal/mol is shown in Fig. 9. The theoretical distribution is in good agreement with experiment for the $v = 1$, 2, and 3 vibrational states giving the same order of their relative population. However, the experimental distribution features a substantial ratio of HF molecules in their ground vibrational state, whereas our simulations provide near-zero relative population for $v = 0$. The same discrepancy with experiment regarding the ground vibrational state was observed for the results of Espinosa-Garcia and co-workers[46] when compared to these experimental data, and in the direct-dynamics work of Layfield *et al.*[37] as well. The latter work also significantly overestimates the $v = 1$ and 2 and underestimates the $v = 3$ populations. This deviation might be caused by the presence of transition-state (Feshbach) resonances,[64–66] a quantum effect not captured by QCT computations, where the excess energy is transferred to other degrees of freedom from the H–F stretching mode near the transition state, making the HF product to be formed in its ground vibrational state. However, the quantum-dynamics studies of Guo and co-workers showed similarly low-populated ground vibrational state for the HF product in the $F + H_2O$ reaction as their QCT studies, in contradiction to experiment.[49,61,67] A similar disagreement between theory and experiment has also been observed in the case of the $F + CH_3CN \rightarrow HF + CH_2CN$ reaction.[68]

The vibrationally-resolved rotational state distributions of HF for the $v = 1$, 2, and 3 vibrational states compared with those of experiment[35] obtained at 3.2 kcal/mol collision energy are plotted in Fig. 10. Excellent agreement is seen for the $v = 2$ and $v = 3$ states, where the experimental data have the lowest error bars,[35] and a rather good agreement is observed also for $v = 1$, considering that the uncertainty of the experimental data increases with a decrease in v.[35] All three rotational distributions, determined both theoretically and experimentally, peak at $J = 2$ and decay more and more sharply with an increase in v. The $v = 0$ rotational distribution is obtained with a significant statistical error from our simulations due to the low relative population of the ground vibrational state, and the experiment also has the largest uncertainty for these data; thus, the comparison is omitted for $v = 0$.

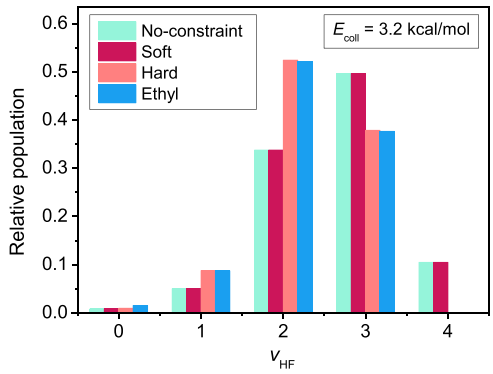

FIG. 8. Vibrational state distribution of the HF product at 3.2 kcal/mol collision energy with different ZPE constraints applied for the products (soft: the sum of the classical vibrational energies of the products is larger than the sum of their ZPEs, hard: the vibrational energy of each product molecule is larger than its ZPE, ethyl: ZPE constraint is set only for the ethyl radical).

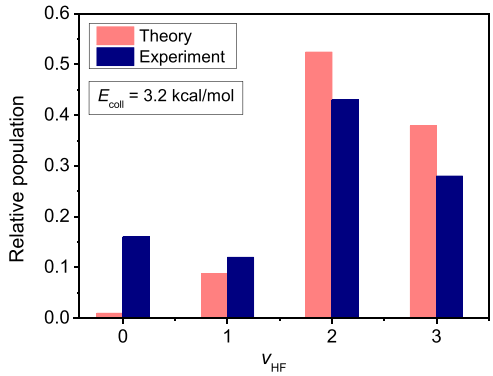

FIG. 9. Vibrational state distribution of the HF product at 3.2 kcal/mol collision energy with hard ZPE constraint (the vibrational energy of each product molecule must be larger than its ZPE) compared to the experimental results taken from Ref. 35.

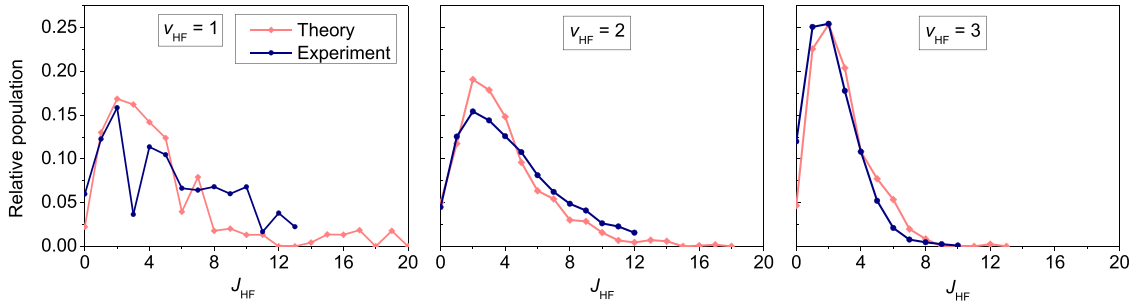

FIG. 10. Normalized vibrationally resolved rotational state distributions of the HF product with hard ZPE constraint (the vibrational energy of each product molecule must be larger than its ZPE) compared to the experimental results taken from Ref. 35 corresponding to the v = 1, 2, and 3 vibrational states of HF at 3.2 kcal/mol collision energy.

IV. CONCLUSIONS

We have developed a full-dimensional multireference spin–orbit-corrected PES for the nine-atomic $F(^2P_{3/2}) + C_2H_6 \rightarrow HF + C_2H_5$ reaction using the ROBOSURFER program package and the monomial symmetrization approach of the permutationally invariant polynomial method for fitting the *ab initio* energy points and studied its dynamics in detail by performing QCT simulations. The MRCI-F12+Q(5,3)/aug-cc-pVDZ level of theory used for the PES development is necessary to correctly describe the entrance channel of the reaction and also reflects well the negative barrier height and the depth of the post-reaction minimum relative to the products; however, its performance is somewhat poorer in the exit-channel. Quasi-classical dynamics simulations on this PES show substantial probabilities of this H-abstraction reaction in a wide range of collision energies, and a sharply rising excitation function, in accordance with its early-barrier nature. Scattering angle distributions of the products indicate a direct rebound mechanism at low collision energies and increasing preference for stripping mechanism as translational energy increases. Relative translational energy distributions of the products and internal energy distributions of the ethyl fragment suggest that most of the collision energy ends up in product translational recoil, and only a slight amount of the initial translational energy excites the rotational–vibrational modes of the ethyl radical. The substantial reaction energy excites the vibration of the HF product owing to the elongated H–F distance at the transition-state geometry, resulting in a vibrational distribution peaking at v = 2, in agreement with experiment. Vibrationally resolved rotational state distributions of the HF molecule obtained from our simulations are compared to the single-collision experimental data, and the results show excellent agreement for the v = 1, 2, and 3 vibrational states. However, discrepancies with experiment are observed regarding the population of the ground vibrational state. The dynamics of the title reaction is also compared to that of the $Cl + C_2H_6 \rightarrow HCl + C_2H_5$ and $F + CH_4 \rightarrow HF + CH_3$ reactions. The accurate theoretical simulation of the present reaction may motivate future experiments and classical or reduced-dimensional quantum dynamics computations.

SUPPLEMENTARY MATERIAL

The supplementary material contains the coefficients and all other necessary files to compute the energies at certain geometries on the newly-developed PES.

ACKNOWLEDGMENTS

We thank the National Research, Development and Innovation Office–NKFIH, K-125317; the Ministry of Human Capacities, Hungary, Grant No. 20391-3/2018/FEKUSTRAT; and the Momentum (Lendület) program of the Hungarian Academy of Sciences for financial support. We acknowledge KIFÜ for awarding us access to computational resources based in Hungary at Budapest and Debrecen. We thank Viktor Tajti for providing technical support in using the MSA program.

DATA AVAILABILITY

The data that support the findings of this study are available from the corresponding authors upon reasonable request and within the supplementary material.

REFERENCES

[1] G. C. Schatz and A. Kuppermann, J. Chem. Phys. **62**, 2502 (1975).
[2] G. C. Schatz and A. Kuppermann, J. Chem. Phys. **65**, 4642 (1976).
[3] G. C. Schatz, J. M. Bowman, and A. Kuppermann, J. Chem. Phys. **63**, 674 (1975).
[4] A. Persky, J. Chem. Phys. **66**, 2932 (1977).
[5] D. Skouteris, J. F. Castillo, and D. E. Manolopoulos, Comput. Phys. Commun. **133**, 128 (2000).
[6] J. C. Polanyi, Science **236**, 680 (1987).
[7] G. C. Schatz, M. C. Colton, and J. L. Grant, J. Phys. Chem. **88**, 2971 (1984).
[8] A. Sinha, M. C. Hsiao, and F. F. Crim, J. Chem. Phys. **92**, 6333 (1990).
[9] M. J. Bronikowski, W. R. Simpson, B. Girard, and R. N. Zare, J. Chem. Phys. **95**, 8647 (1991).
[10] R. B. Metz, J. D. Thoemke, J. M. Pfeiffer, and F. F. Crim, J. Chem. Phys. **99**, 1744 (1993).
[11] D. H. Zhang and J. C. Light, J. Chem. Soc., Faraday Trans. **93**, 691 (1997).
[12] J. P. Camden, H. A. Bechtel, and R. N. Zare, Angew. Chem., Int. Ed. **42**, 5227 (2003).
[13] Z. H. Kim, A. J. Alexander, H. A. Bechtel, and R. N. Zare, J. Chem. Phys. **115**, 179 (2001).
[14] S. Yoon, S. Henton, A. N. Zivkovic, and F. F. Crim, J. Chem. Phys. **116**, 10744 (2002).
[15] J. J. Lin, J. Zhou, W. Shiu, and K. Liu, Science **300**, 966 (2003).
[16] S. Yan, Y.-T. Wu, B. Zhang, X.-F. Yue, and K. Liu, Science **316**, 1723 (2007).
[17] W. Zhang, H. Kawamata, and K. Liu, Science **325**, 303 (2009).
[18] F. Wang, J.-S. Lin, and K. Liu, Science **331**, 900 (2011).
[19] D. Troya, J. Chem. Phys. **123**, 214305 (2005).
[20] J. Espinosa-García, J. L. Bravo, and C. Rangel, J. Phys. Chem. A **111**, 2761 (2007).

[21] G. Czakó, B. C. Shepler, B. J. Braams, and J. M. Bowman, J. Chem. Phys. **130**, 084301 (2009).
[22] G. Czakó and J. M. Bowman, Phys. Chem. Chem. Phys. **13**, 8306 (2011).
[23] G. Czakó and J. M. Bowman, Science **334**, 343 (2011).
[24] G. Czakó and J. M. Bowman, Proc. Natl. Acad. Sci. U. S. A. **109**, 7997 (2012).
[25] G. Czakó, J. Chem. Phys. **138**, 134301 (2013).
[26] G. Czakó and J. M. Bowman, J. Phys. Chem. A **118**, 2839 (2014).
[27] F. Meng, W. Yan, and D. Wang, Phys. Chem. Chem. Phys. **14**, 13656 (2012).
[28] N. Liu and M. Yang, J. Chem. Phys. **143**, 134305 (2015).
[29] B. Fu, X. Shan, D. H. Zhang, and D. C. Clary, Chem. Soc. Rev. **46**, 7625 (2017).
[30] S. A. Kandel, T. P. Rakitzis, T. Lev-On, and R. N. Zare, J. Chem. Phys. **105**, 17 (1996).
[31] C. Murray and A. J. Orr-Ewing, Int. Rev. Phys. Chem. **23**, 435 (2004).
[32] C. Murray, J. K. Pearce, S. Rudić, B. Retail, and A. J. Orr-Ewing, J. Phys. Chem. A **109**, 49 (2005).
[33] N. Balucani, G. Capozza, F. Leonori, E. Segoloni, and P. Casavecchia, Int. Rev. Phys. Chem. **25**, 109 (2006).
[34] C. Huang, W. Li, and A. G. Suits, J. Chem. Phys. **125**, 133107 (2006).
[35] E. S. Whitney, A. M. Zolot, A. B. McCoy, J. S. Francisco, and D. J. Nesbitt, J. Chem. Phys. **122**, 124310 (2005).
[36] S. J. Greaves, J. Kim, A. J. Orr-Ewing, and D. Troya, Chem. Phys. Lett. **441**, 171 (2007).
[37] J. P. Layfield, A. F. Sweeney, and D. Troya, J. Phys. Chem. A **113**, 4294 (2009).
[38] D. Papp, V. Tajti, T. Győri, and G. Czakó, J. Phys. Chem. Lett. **11**, 4762 (2020).
[39] D. Papp, B. Gruber, and G. Czakó, Phys. Chem. Chem. Phys. **21**, 396 (2019).
[40] A. Persky, Chem. Phys. Lett. **380**, 286 (2003).
[41] G. C. Fettis, J. H. Knox, and A. F. Trotman-Dickenson, J. Chem. Soc. **1960**, 1064 (1960).
[42] R. Foon and G. P. Reid, Trans. Faraday Soc. **67**, 3513 (1971).
[43] M. M. Maricq and J. J. Szente, J. Phys. Chem. **98**, 2078 (1994).
[44] O. Roberto-Neto and F. B. C. Machado, Chem. Phys. Lett. **449**, 67 (2007).
[45] J. Espinosa-Garcia, J. C. Corchado, M. Garcia-Chamorro, and C. Rangel, Phys. Chem. Chem. Phys. **20**, 19860 (2018).
[46] J. Espinosa-Garcia and M. Garcia-Chamorro, Phys. Chem. Chem. Phys. **20**, 26634 (2018).
[47] J. Espinosa-Garcia, M. Garcia-Chamorro, J. C. Corchado, S. Bhowmick, and Y. V. Suleimanov, Phys. Chem. Chem. Phys. **22**, 13790 (2020).
[48] M. P. Deskevich, D. J. Nesbitt, and H.-J. Werner, J. Chem. Phys. **120**, 7281 (2004).
[49] J. Li, R. Dawes, and H. Guo, J. Chem. Phys. **137**, 094304 (2012).
[50] H.-J. Werner and P. J. Knowles, J. Chem. Phys. **89**, 5803 (1988).
[51] T. H. Dunning, Jr., J. Chem. Phys. **90**, 1007 (1989).
[52] A. Berning, M. Schweizer, H.-J. Werner, P. J. Knowles, and P. Palmieri, Mol. Phys. **98**, 1823 (2000).
[53] S. R. Langhoff and E. R. Davidson, Int. J. Quantum Chem. **8**, 61 (1974).
[54] H.-J. Werner, P. J. Knowles, G. Knizia, F. R. Manby, M. Schütz *et al.*, MOLPRO, version 2015.1, a package of *ab initio* programs, see http://www.molpro.net.
[55] T. Győri and G. Czakó, J. Chem. Theory Comput. **16**, 51 (2020).
[56] Z. Xie and J. M. Bowman, J. Chem. Theory Comput. **6**, 26 (2010).
[57] B. J. Braams and J. M. Bowman, Int. Rev. Phys. Chem. **28**, 577 (2009).
[58] J. M. Bowman, G. Czakó, and B. Fu, Phys. Chem. Chem. Phys. **13**, 8094 (2011).
[59] W. L. Hase, *Encyclopedia of Computational Chemistry* (Wiley, New York, 1998), pp. 399–407.
[60] G. S. Hammond, J. Am. Chem. Soc. **77**, 334 (1955).
[61] J. Li and H. Guo, Chin. J. Chem. Phys. **26**, 627 (2013).
[62] B. Jiang and H. Guo, J. Am. Chem. Soc. **135**, 15251 (2013).
[63] D. M. Neumark, A. M. Wodtke, G. N. Robinson, C. C. Hayden, and Y. T. Lee, J. Chem. Phys. **82**, 3045 (1985).
[64] A. M. Zolot and D. J. Nesbitt, J. Chem. Phys. **127**, 114319 (2008).
[65] R. T. Skodje, D. Skouteris, D. E. Manolopoulos, S.-H. Lee, F. Dong, and K. Liu, J. Chem. Phys. **112**, 4536 (2000).
[66] M. Qiu, Z. F. Ren, L. Che, D. Dai, S. A. Harich, X. Wang, X. Yang, C. Xu, D. Xie, M. Gustafsson, R. T. Skodje, Z. Sun, and D. H. Zhang, Science **311**, 1440 (2006).
[67] B. Zhao and H. Guo, J. Phys. Chem. Lett. **6**, 676 (2015).
[68] S. Pratihar, X. Ma, J. Xie, R. Scott, E. Gao, B. Ruscic, A. J. A. Aquino, D. W. Setser, and W. L. Hase, J. Chem. Phys. **147**, 144301 (2017).